PNAS RESEARCH ARTICLE | ANTHROPOLOGY

The reconstructed cranium of *Pierolapithecus* and the evolution of the great ape face

Kelsey D. Pugh[a,b,c,1], Santiago A. Catalano[d,e], Miriam Pérez de los Ríos[f], Josep Fortuny[g], Brian M. Shearer[c,h,i], Alessandra Vecino Gazabón[b,c,j], Ashley S. Hammond[b,c], Salvador Moyà-Solà[g,k,l], David M. Alba[g], and Sergio Almécija[b,c,g]

Edited by Christoph P. Zollikofer, Universitat Zurich, Zurich, Switzerland; received November 3, 2022; accepted August 29, 2023 by Editorial Board Member C. O. Lovejoy

Pierolapithecus catalaunicus **(~12 million years ago, northeastern Spain) is key to understanding the mosaic nature of hominid (great ape and human) evolution. Notably, its skeleton indicates that an orthograde (upright) body plan preceded suspensory adaptations in hominid evolution. However, there is ongoing debate about this species, partly because the sole known cranium, preserving a nearly complete face, suffers from taphonomic damage. We 1) carried out a micro computerized tomography (CT) based virtual reconstruction of the *Pierolapithecus* cranium, 2) assessed its morphological affinities using a series of two-dimensional (2D) and three-dimensional (3D) morphometric analyses, and 3) modeled the evolution of key aspects of ape face form. The reconstruction clarifies many aspects of the facial morphology of *Pierolapithecus*. Our results indicate that it is most similar to great apes (fossil and extant) in overall face shape and size and is morphologically distinct from other Middle Miocene apes. Crown great apes can be distinguished from other taxa in several facial metrics (e.g., low midfacial prognathism, relatively tall faces) and only some of these features are found in *Pierolapithecus*, which is most consistent with a stem (basal) hominid position. The inferred morphology at all ancestral nodes within the hominoid (ape and human) tree is closer to great apes than to hylobatids (gibbons and siamangs), which are convergent with other smaller anthropoids. Our analyses support a hominid ancestor that was distinct from all extant and fossil hominids in overall facial shape and shared many features with *Pierolapithecus*. This reconstructed ancestral morphotype represents a testable hypothesis that can be reevaluated as new fossils are discovered.**

fossil apes | great apes | face morphometrics | evolution

Significance

One of the persistent issues in studies of ape and human evolution is that the fossil record is fragmentary and many specimens are incompletely preserved and/or distorted. This makes it difficult to reach a consensus on the evolutionary relationships of key fossil apes that are essential to understanding ape and human evolution. Here, we reconstruct the face of *Pierolapithecus catalaunicus* and analyze its morphology in an evolutionary framework. Our results are consistent with the hypothesis that this species represents a basal member of the group including great apes and humans, and provide insight into the facial morphology of the ancestor of the group.

The morphological and taxonomic diversity of hominoids (apes and humans) in the Miocene of Europe has expanded since the turn of the century with the discovery of new specimens and the description of new genera and species (1–4). Of the eight widely recognized genera, three (*Dryopithecus*, *Anoiapithecus*, and *Pierolapithecus*) are found at different Middle Miocene localities (ranging from 12.4 to 11.9 million years ago [Ma]) within a single site called Abocador de Can Mata (ACM) in northeastern Spain. The ACM hominoids preserve interesting combinations of primitive and derived features that are critical to bettering our understanding of the origin and evolution of hominids (great apes and humans). *Pierolapithecus*, in particular, has played a central role in discussions of hominoid locomotor evolution because it has features of the lumbar vertebrae, ribs, and hip that are indicative of an orthograde (upright) body plan (present in all extant hominoids), but it has been argued to lack specific adaptations to suspensory locomotion, such as long, curved phalanges (1, 5–7, but see ref. 8). The latter are present in all extant apes (nonhuman hominoids: chimpanzees, bonobos, gorillas, orangutans, and hylobatids) except in the larger and more terrestrial gorilla species, which are widely considered as secondarily derived in this respect (but see ref. 9). Hence, this combination of postcranial features in *Pierolapithecus* gives support to the hypothesis that the evolution of an orthograde body plan and suspension were decoupled in hominoid evolution and that adaptations for suspension evolved independently in some hominoid lineages (1, 5, 7, 10). However, evolutionary interpretations of these morphologies and behaviors are reliant on underlying phylogenetic relationships, necessitating a clear understanding of how *Pierolapithecus* relates to other European and extant hominoids.

Most authors agree that the majority of European hominoids (or "dryopiths"), including *Pierolapithecus*, represent members of the hominid clade, although there is disagreement over their precise placement within the clade (reviewed in ref. 11). They have been hypothesized to be more closely related to African apes and humans (hominines) (e.g., refs. 12 and 13) or to orangutans (pongines) (e.g., refs. 10 and 14), or to precede the divergence of these clades (i.e., stem hominids; stem taxa are those members of a clade that branch before the node representing the last common ancestor (LCA) of extant members, which

Author contributions: K.D.P. and S.A. designed research; K.D.P., J.F., B.M.S., S.M.-S., and D.M.A. carried out the virtual reconstruction and imaging; K.D.P. and A.V.G. collected data; K.D.P., S.A.C., and S.A. analyzed data; K.D.P., S.A.C., M.P.d.l.R., J.F., B.M.S., A.V.G., A.S.H., S.M.-S., D.M.A., and S.A. discussed and interpreted results; K.D.P. wrote the paper with feedback from S.A.C., M.P.d.l.R., J.F., B.M.S., A.V.G., A.S.H., S.M.-S., D.M.A., and S.A.

The authors declare no competing interest.

This article is a PNAS Direct Submission. C.P.Z. is a guest editor invited by the Editorial Board.

[1]To whom correspondence may be addressed. Email: kelsey.pugh@brooklyn.cuny.edu.

This article contains supporting information online at https://www.pnas.org/lookup/suppl/doi:10.1073/pnas.2218778120/-/DCSupplemental.

Published October 16, 2023.

defines the crown group) (e.g., refs. 15 and 16). A recent comprehensive cladistic analysis of hominids found support for the latter position for Middle and early Late Miocene European hominoids (17). In addition to the debate about how European hominoids are related to extant hominoids, the relationships among them are poorly understood (17) and there are ongoing debates about their taxonomy. The hominoids from ACM have been distinguished from one another primarily on the basis of craniofacial morphology (2, 3), although differences in dental morphology between both *Pierolapithecus* and *Anoiapithecus* compared to *Dryopithecus* have also been noted (3, 18–21). However, the close stratigraphic and geographic proximity of the ACM hominoid fossils, in combination with other factors, has led some authors to question their distinctiveness (e.g., refs. 13, 22, and 23).

One of the primary complications in evaluating the systematics of these hominoids stems from taphonomic damage to cranial fossils. Deformation and incomplete preservation hinder comprehensive anatomical comparisons and contribute to differing interpretations of anatomical features and overall morphology by different authors. The holotype cranium of *Pierolapithecus* (IPS21350.1), associated with a partial skeleton of an adult male, preserves a remarkably complete, although partially distorted, craniofacial skeleton (1). As a result of damage to the cranium, the description and interpretation of this specimen have been critiqued (13, 22, 23). To better understand the evolutionary role of *Pierolapithecus*, we undertook a microCT-based virtual reconstruction of the holotype cranium, which corrects for major distortions and facilitates a better understanding of its facial morphology. Subsequently, we analyzed the reconstructed cranium in the context of a broad anthropoid comparative sample using linear and 3D geometric morphometrics to quantitatively assess its morphological affinities. We then reconstructed the facial morphology for ancestral nodes in the hominoid tree—including the LCA of all hominids—using phylogenetic comparative methods and modeled its evolution.

Results

The Reconstruction of IPS21350.1. The facial skeleton of the *Pierolapithecus catalaunicus* holotype is remarkably complete, although it suffers from deformation and there is some bone missing from the maxilla on both sides in the region of the nasal aperture, zygomatic processes, and canine alveoli. The face was found largely in one piece (*SI Appendix*, Fig. S1), with several fragments that were broken away during recovery and discovered as detached fragments, including the premaxilla, the canines, an inferolateral fragment of the right zygomatic, and several maxillary fragments, including a previously undocumented fragment of the left maxilla preserving part of the lateral margin of the nasal aperture (Fig. 1 *A*–*C*). Except for the latter, each of these can be refit on the cranium with confidence. The left maxillary fragment is difficult to refit due to distortion resulting from crushing and expansion caused by matrix infilling. The nasal aperture is filled with matrix, and cemented mixtures of small bone fragments and matrix are adhered to the cranium in several places (*SI Appendix*, Figs. S1 and S2 and *Extended Description*). Evaluation of CT scans reveals that the primary distortion of the *Pierolapithecus* holotype cranium results from fragmentation and displacement rather than plastic deformation, which can thus be corrected by virtually separating and repositioning the fragments.

We virtually segmented major fragments along fractures and from matrix infill on CT scans (Fig. 1 *D* and *E*). Following segmentation, we carried out a single virtual reconstruction of the specimen, which consisted of repositioning and mirroring of displaced fragments. The bones of the upper (zygomatics and orbital/supraorbital regions) and lower (palate) face were repositioned separately, and subsequently, the upper face block was reoriented relative to the lower face based on the alignment of the zygomatic roots of the maxillae and the zygomatics, as well as the alignment of the nasal aperture margin as indicated by the preserved region on the premaxilla and the detached maxillary fragment (*SI Appendix, Extended Methods*). Displacement between these regions is evident on the original specimen, with the upper face forming an unnatural angle relative to the palate (Fig. 1*A*). We quantified the orientation of the upper face relative to the lower face by measuring the angle between the orbits and the alveolar plane. The unreconstructed cranium has a very low orbit angle (L: 50.3°; R: 46.6°), well below that of any fossil or extant anthropoid in our sample (58.2 to 96.0°; *SI Appendix*, Fig. S3). The reconstruction has a higher orbit angle (64°) that falls within the lower part of the range of variation of our comparative sample. The final reconstruction is shown in Fig. 1 *G*–*I*, and selected cranial measurements are provided in *SI Appendix*, Table S1.

3D Shape and Size of the Hominoid Face. The correction of the distortions of IPS21350.1 makes it possible to directly compare this cranium to other extant and fossil anthropoids quantitatively by applying 3D geometric morphometrics. We used sixty-seven landmarks (*SI Appendix*, Fig. S4 and Table S2) to study the overall shape affinities of the face of *Pierolapithecus* within a comparative sample of extant and fossil anthropoids (n = 80; *SI Appendix*, Tables S3 and S4). Landmarks were selected based on preservation in *Pierolapithecus*, but also to maximize the inclusion of other fossil hominoids in the sample. Still, a limited number of fossil specimens could be included. A second iteration with a reduced landmark set capturing the lower half of the face (53 landmarks; *SI Appendix*, Fig. S4) was performed so that the distorted cranium of *Ekembo*, an important stem hominoid taxon from the Early Miocene, could be included (*SI Appendix*, Figs. S5–S8 and *Extended Results*).

We examined the patterns of face shape and size variation in anthropoids using principal components analysis (PCA) of Procrustes-aligned coordinates and centroid size (CS) (Fig. 2 and *SI Appendix*, Fig. S9). We employed thin-plate spline (TPS) warping to easily visualize the morphological differences in the sample as captured by the extremes of variation along PC1–PC3. The combination of PC1 and PC2 (Fig. 2*A*), which account for 50.6% and 11.2% of the shape variation in the sample (respectively), separates all extant and fossil great apes from hylobatids and monkeys. On PC1, the major shape changes relate primarily to relative face length (prognathism) and height. The relationship of the orbits and nasal aperture in the superoinferior plane, which contributes to overall facial height, and the orientation of the infraorbital region are also captured. *Epipliopithecus*, with its superoinferiorly short, orthognathic (flat) face, sits at the negative extreme of the axis, and *Papio*, with its very prognathic and tall face, sits at the positive extreme of the axis. Great ape shape space overlaps with cercopithecoid shape space on PC1, especially due to the divergent position of *Papio*. Of the sampled cercopithecoids, only *Colobus* overlaps with hylobatids and platyrrhines on the negative end of PC1. *Epipliopithecus* is the only fossil that occupies a position on the negative end of the PC1 axis, falling closest to *Hylobates*.

On PC2, the major shape changes reflected in the TPS warps relate to midfacial prognathism, nasal aperture shape, and clivus length. *Papio*, with its elongated snout, sits at the negative extreme of the axis, while *Pan paniscus* and *Sivapithecus*, which have very low midfacial prognathism, sit at the positive extreme. Among great apes, *Gorilla* and *Pongo* overlap extensively and occupy an

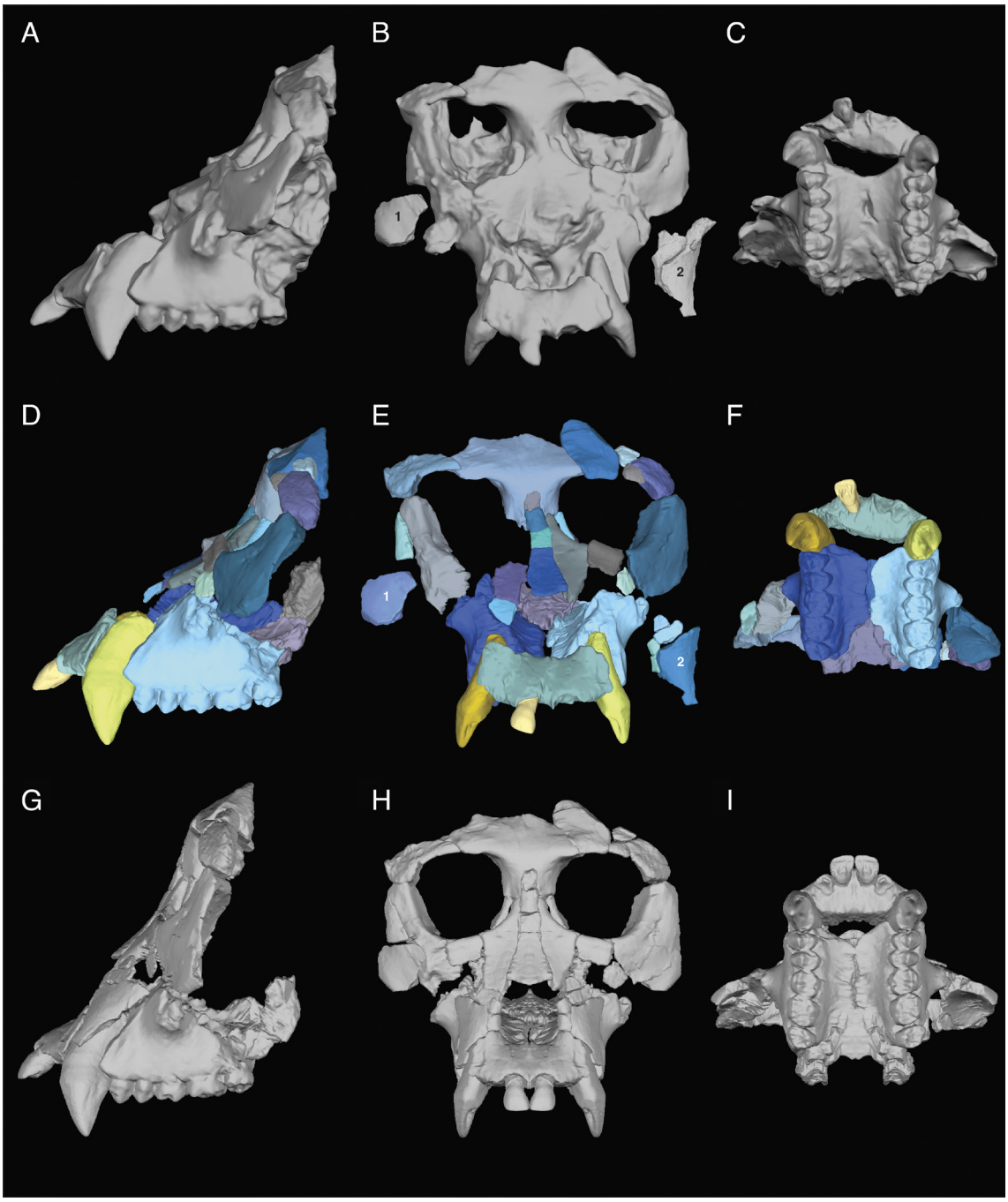

Fig. 1. Cranium of *P. catalaunicus* (IPS21350.1, holotype) in lateral (left column), anterior (middle column), and inferior (right column) views. (*A–C*) Surface scan of original fossil; (*D* and *E*) segmentation; (*G–I*) reconstruction. Fragments 1 and 2, along with the canines and premaxilla, were found as detached fragments.

intermediate position between cercopithecoids and *Pan* on PC2. *Aegyptopithecus*, *Victoriapithecus*, and *Afropithecus* are closest to cercopithecoids (*Macaca* and *Nasalis*) and *Sivapithecus* is closest to *Gorilla* and *Pongo* when both PC1 and PC2 are considered, occupying a more positive position on PC1 due to its very superoinferiorly elongated face (see also Fig. 5*A*). GSP 15000 was found in several pieces, so the height of the face may be influenced by the relative placement of these fragments in the reconstruction used here (see *SI Appendix*, Table S4 for details) and/or by deformation (24). However, some previous analyses of GSP 15000 have also found it to fall outside the range of variation of *Pongo* and other extant great apes (e.g., ref. 2).

Pierolapithecus and *Anoiapithecus* occupy positions very near to each other, with *Anoiapithecus* falling just within *Pongo* and very near to *Gorilla* and *Pierolapithecus* just outside of, but in close proximity to, the shape space of all three extant great ape genera. The high position of the orbits relative to the nasal aperture in *Anoiapithecus* may contribute to its slightly more positive position on PC1 than *Pierolapithecus*, despite its very orthognathic face. *Pierolapithecus* and *Anoiapithecus* are more distant from one another on PC3 (6.8% of the variation; *SI Appendix*, Fig. S9). When all taxon-averaged Procrustes distances (with or without lnCS) are summarized using a UPGMA cluster analysis, *Pierolapithecus* clusters first with *Anoiapithecus* (*SI Appendix*, Fig. S10).

To maximize the within great ape differences, we also repeated the PCA and UPGMA with a reduced taxon sample that included only extant great apes and fossil hominoids (*SI Appendix*, Figs. S11

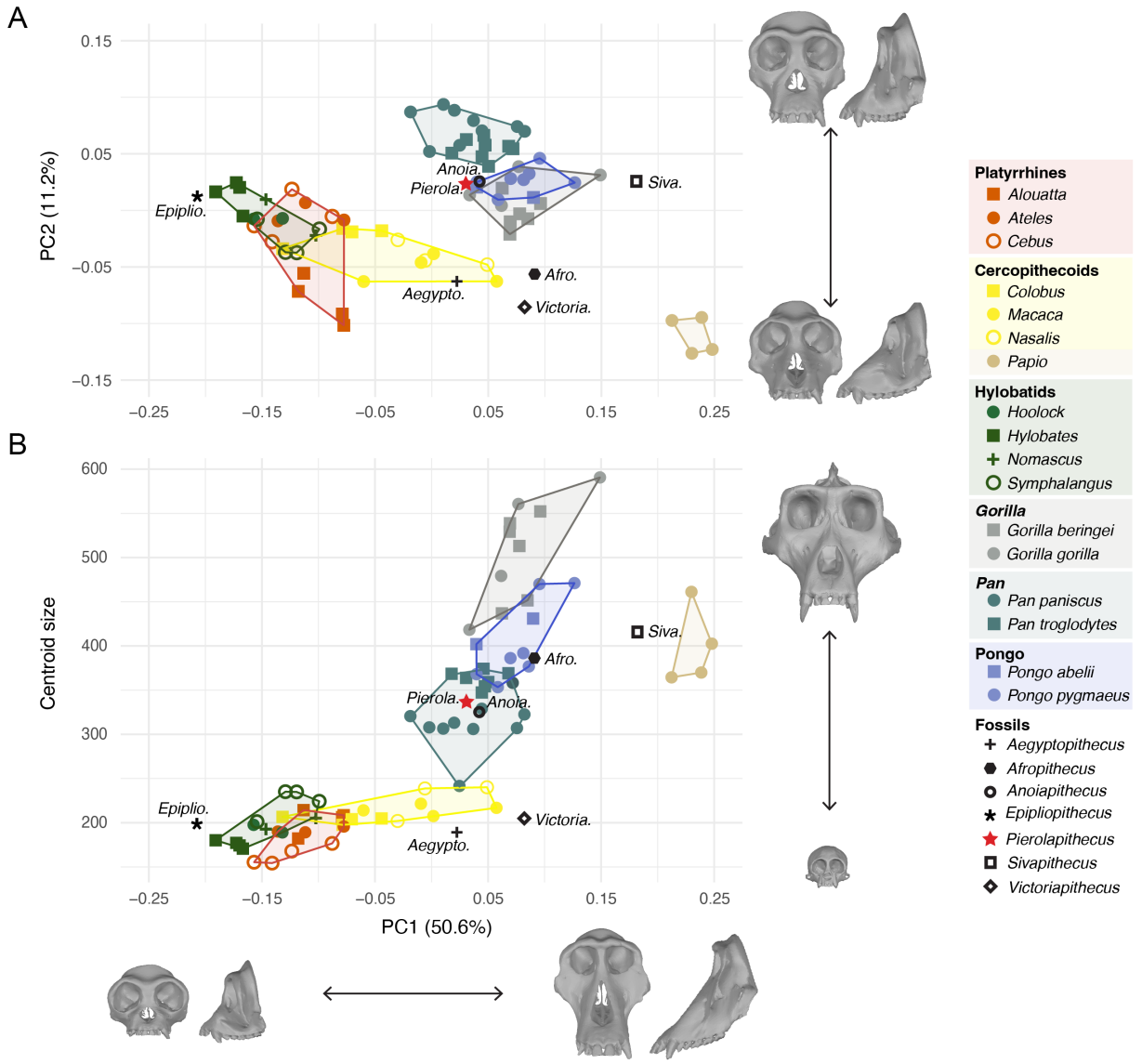

Fig. 2. Anthropoid shape and shape-size spaces: (*A*) PC 1 and 2; (*B*) PC1 and face CS in millimeters (mm) calculated from 67 landmarks. Due to its divergent position from other cercopithecoids, *Papio* is visualized in a separate polygon. Models along the PC axes are TPS warps of the mean specimen (AMNH 89406, *Pan troglodytes*) representing the positive and negative extremes of each axis. Models on the CS axis in *B* are the smallest (USNM 397940, *Cebus*) and largest (CMNH 2767, *Gorilla*) specimens in the sample, to scale.

and S12 and *Extended Results*). There is overlap among extant great apes on each of these axes, but when PC1 (28.9% of shape variation in the sample) is visualized with PC2 (14.4% of shape variation in the sample) or PC3 (11.9% of shape variation in the sample), the overlap is minimal compared to when the whole taxon sample is analyzed. When PC1 and PC2 are visualized together, *Anoiapithecus* falls in *Pongo* shape space, *Afropithecus* falls with *Gorilla*, and *Pierolapithecus* falls in the space between the three extant great ape genera, but closest to *Gorilla*. *Sivapithecus* does not overlap with any extant taxon but sits at the negative extreme of PC1 and the positive extreme of PC2. In the UPGMA trees, *Pierolapithecus* again clusters with *Anoiapithecus*. Overall, these reduced taxon sample analyses do not provide additional insights into the affinities of *Pierolapithecus*.

Since some of the shape changes along PC1 appear to be related to overall size, with smaller taxa (e.g., platyrrhines, hylobatids, and *Epipliopithecus*) on the negative end of PC1 and larger taxa (e.g., *Gorilla* and *Papio*) on the positive end, we evaluated the relationship of overall face shape (PC1 scores) and CS (i.e., allometry) in a bivariate plot (Fig. 2*B*) and a pGLS (phylogenetic generalized least squares; see below). This plot separates extant groups reasonably well. There is a clear difference in face size between extant great apes and other extant anthropoids except for *Papio*, which falls in the great ape range. In general, larger face size is associated with higher values on PC1, but shape does not closely track size because, in many cases, specimens that are similar in face size differ greatly in shape (e.g., *Papio* falls within the range of great apes in face size but is distinct in shape; one very small *Pan paniscus* specimen [AMNH 86857] is in the size range of male *Nasalis* but falls in the middle of the range of shape variation for *Pan*), and specimens that are similar in shape differ in size (e.g., extant great apes overlap with *Macaca*, *Nasalis*, *Victoriapithecus*, and *Aegyptopithecus* in face shape despite differences in size). Among non-*Papio* monkeys and hylobatids, there is very little variation in face size, especially compared to the wide range of variation observed in great apes. Fossil hominoids fall in the size range of great apes (*Pan* and *Pongo*, specifically), with *Pierolapithecus* intermediate in size between *Pan paniscus* and *Pan troglodytes*. The overlap of some extant monkeys with great

apes on PC1 despite differences in face size indicates that the gross facial shape differences between great apes and the rest of the sample are not merely attributable to size differences.

Evolutionary Modeling of Hominoid Facial Form. Next, to better understand major changes in face shape during anthropoid evolution, we enlisted a 3D phylomorphospace approach using the same 67 landmark dataset by performing a PCA on Procrustes-aligned mean coordinates for each genus (with the exception of *Pan,* for which means were calculated for each species to preserve important known differences in both cranial shape and size). This method projects a time-calibrated phylogenetic tree (with *Pierolapithecus* positioned as a stem hominid based on 17) into morphospace and reconstructs the position of ancestral nodes [using maximum likelihood (ML), in this case], thereby allowing for visualization of the inferred direction and extent of the shape changes along each branch between reconstructed internal nodes and tips (*Materials & Methods*). The first three PCs, which account for 75.7% of shape variation in the sample, were used (Fig. 3). For clarity, 2D phylomorphospace plots with TPS warps depicting the shapes at the most extreme points along the PC1–PC3 axes are also presented in *SI Appendix*, Fig. S13. The phylomorphospaces based on means show no appreciable differences in pattern when compared to the PCA performed on individual specimens. An underlying phylogenetic structure in overall shape, individual PCs (PC1-3), and CS was detected (*SI Appendix*, Table S5). The reconstructed 3D shape of the ancestor of all hominids is shown in *SI Appendix*, Fig. S14.

When the first three PCs are examined together in the 3D phylomorphospace, stem and crown hominids, including *Pierolapithecus*, are set apart from other taxa. The reconstructed hominoid, crown hominoid, and hominid nodes sit near this cluster. Hylobatids diverge from other hominoid taxa and nodes and overlap in shape space with platyrrhines (*Cebus* and *Ateles*) and near to *Epipliopithecus*. The putative stem hominoid *Afropithecus* occupies a position much closer to hominids than to hylobatids. Taken together, these results indicate that 1) the stem and crown hominoid ancestors were more like extant great apes than extant hylobatids in face shape, and 2) that the facial morphology of hylobatids is convergent with that of platyrrhines and *Epipliopithecus*. Convergence in shape among these taxa may result, in part, from secondary reduction in face size in hylobatids and *Epipliopithecus*, as evidenced by a phylomorphospace constructed from PC1 and CS (Fig. 4). This plot shows that smaller taxa that converge on a similar face shape have each evolved from an ancestor with a larger face. pGLS regression results of PC1 and lnCS indicate that there is a significant allometric trend between these two variables associated with ~50% of the shape variation captured by PC1 (R^2: 0.4948; *P*-value: 0.0001).

Within the hominid clade, *Gorilla* falls nearest to the reconstructed ancestral hominid node. *Pongo* occupies a position near *Gorilla*, and *Sivapithecus* is distinct from all other taxa in the 3D phylomorphospace. *Pierolapithecus* and *Anoiapithecus* are closest to *Pan paniscus* and *Pan troglodytes* but diverge on PC3. Cercopithecoids (excluding *Papio*), along with the inferred cercopithecoid, crown catarrhine, catarrhine, and anthropoid ancestral nodes, partially bridge the gap between the hominid and hylobatid/platyrrhine clusters on PC1. Within cercopithecoids, *Macaca* and *Nasalis* occupy positions closest to the reconstructed ancestral cercopithecoid node, while *Colobus*, *Victoriapithecus*, and *Papio* have diverged

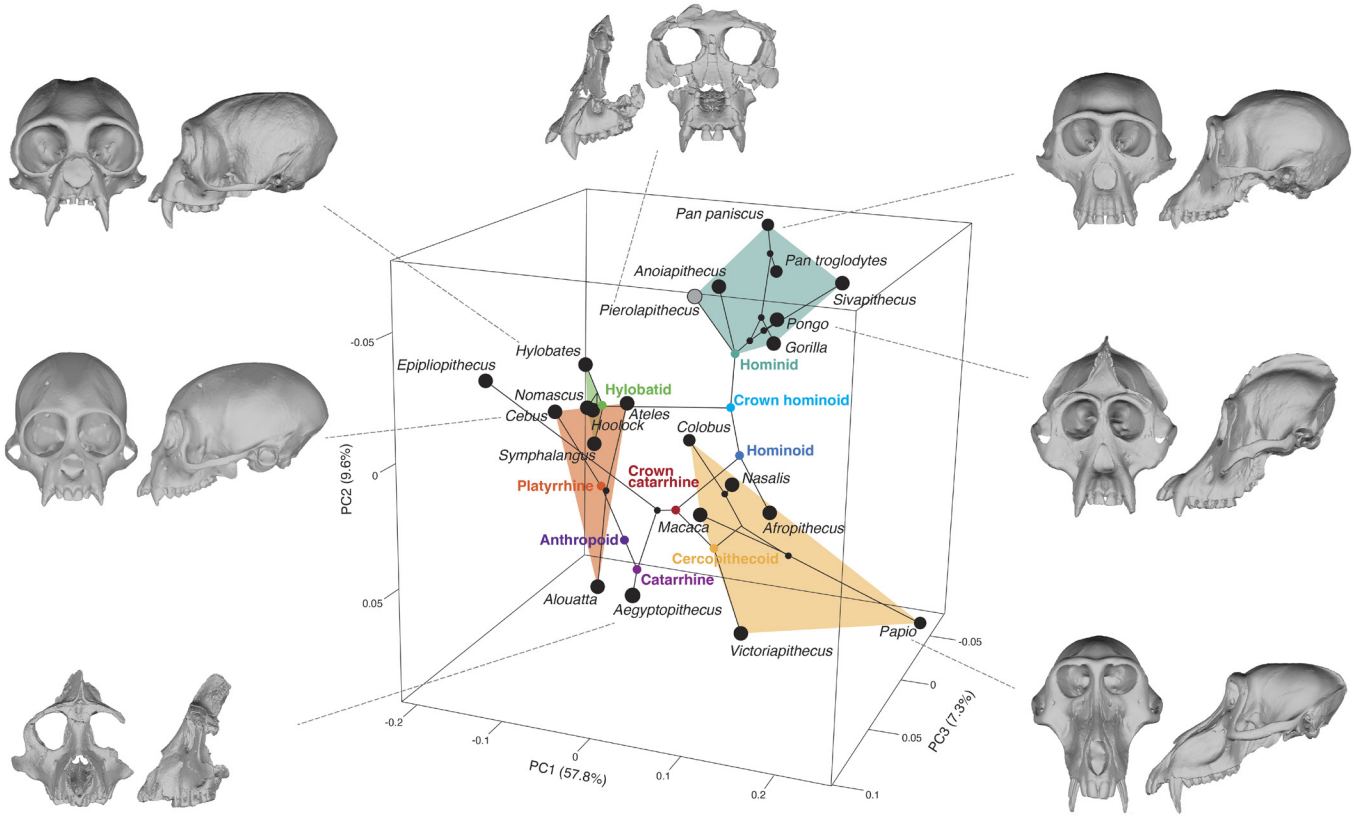

Fig. 3. 3D phylomorphospace showing the inferred evolutionary history of anthropoid facial shape. The three dimensions represent PC 1, 2, and 3 of a PCA on Procrustes-aligned mean coordinates for each taxon. Extant representatives of each major clade (Hominidae, Hylobatidae, Platyrrhini, and Cercopithecoidea) are shown in anterior and lateral views, as well as the stem catarrhine *Aegyptopithecus* and the reconstruction of *Pierolapithecus*. Polygons around hominid, hylobatid, cercopithecid, and platyrrhine shape space are colored according to the color of each node marker. The extant specimens show the entire cranium, but only the face shape has been captured by the landmarks (*SI Appendix*, Table S2 and Fig. S4). Counter clockwise from top: *Pierolapithecus* (reconstruction of IPS 21350.1), *Hylobates* (AMNH 103347), *Cebus* (AMNH 245697), *Aegyptopithecus* (DPC 2803), *Papio* (AMNH 51380), *Pongo* (NMNH 145301), and *Pan paniscus* (MCZ 38020).

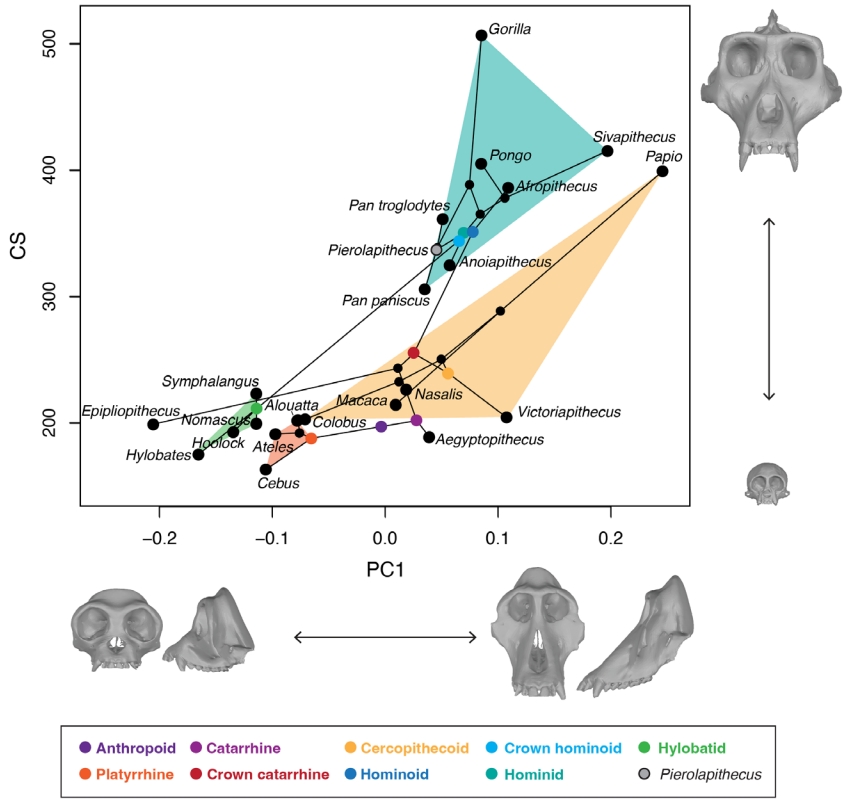

Fig. 4. Shape (PC1) and size (CS in mm) phylomorphospace for the full landmark dataset showing reconstructed evolutionary history of anthropoid cranial shape and size. Reconstructed ancestral nodes are colored according to the legend at *Bottom*. Polygons around hominid, hylobatid, cercopithecid, and platyrrhine shape-size space are also colored according to this legend. Models along the PC1 axis are TPS warps of the mean specimen (AMNH 89406, *Pan troglodytes*) representing the positive and negative extremes of the axis. Models on the CS axis are the smallest (USNM 397940, *Cebus*) and largest (CMNH 2767, *Gorilla*) specimens in the sample, to scale.

further and in different directions. *Colobus* occupies a position closer to hylobatids and platyrrhines, while *Papio* is separated from all other taxa. *Aegyptopithecus* is the taxon closest in face shape to the inferred catarrhine LCA, while *Epipliopithecus* is highly divergent in the direction of hylobatids and some platyrrhines. Within platyrrhines, *Alouatta* diverges from the platyrrhine node to a position nearer to *Aegyptopithecus* in the 3D phylomorphospace.

Since our taxonomic sample is necessarily restricted to those stem catarrhine and hominoids preserving relatively complete faces, which represent a small proportion of currently known taxa, we have performed several additional sensitivity analyses to evaluate the stability of these results. First, phylomorphospaces were constructed with a reduced landmark dataset that permitted the inclusion of *Ekembo*. The addition of further stem hominoids is especially important in reconstructing the shape and size of the hominoid and crown hominoid nodes because stem hominoids are morphologically diverse. These analyses produced a similar pattern as the full dataset (*SI Appendix*, Figs. S7 and S8 and *Extended Results*). For example, the addition of *Ekembo* shifts the hominoid LCA slightly toward hylobatids on the PC1 and CS axes, but the reconstructed hominoid node is still closer to great apes than to hylobatids. Second, we also modeled the evolution of molar size (measured as the square root of M^1 area) on a larger taxonomic sample as a proxy for body size evolution (*SI Appendix*, Fig. S15). The result of this analysis also supports the hypothesis that there was a secondary reduction in size in hylobatids and some stem hominoid taxa.

Evolution of other hominoid facial traits. In addition to 3D geometric morphometric analyses of overall face shape, we also investigated inter- and intraspecific variation in continuous features that were clarified by the reconstruction of the *Pierolapithecus* cranium or have been central in previous discussion of hominoid evolution. Like in the case of overall face shape and size, we modeled the evolutionary history of these features using ML (assuming Brownian motion) ancestral state reconstruction (ASR) and calculated phylogenetic signal (K and λ) for each trait (*SI Appendix*, Table S5). Features include 1) face shape (face height [distance between a point immediately superior to glabella and the alveolar plane]/face breadth), 2) overlap of the nasal aperture and orbits (height of orbit/height of rhinion), 3) relative midfacial prognathism (midfacial prognathism [distance between rhinion and a bi-orbital plane]/CS), 4) relative subnasal clivus length (subnasal clivus length [distance from nasospinale to prosthion]/CS), 5) relative interorbital breadth (interorbital breadth/CS), 6) orbital shape (orbit height/orbit breadth), 7) relative nasal aperture breadth (nasal aperture breadth/CS), and 8) nasal aperture angle (angle between the nasal aperture plane and the alveolar plane) (Fig. 5 and *SI Appendix*, Figs. S16–S20 and Table S6).

Relative to other extant anthropoids, great apes are derived for several of these features. They have taller faces relative to breadth (Fig. 5*A*), orbits that sit higher on the face relative to the nasal aperture (Fig. 5*B*), low midfacial prognathism (Fig. 5*C*), and elongated subnasal clivi (*SI Appendix*, Fig. S16). These features each have high phylogenetic signal (as measured by K and/or λ). *Pierolapithecus* shares the derived condition for overlap of the nasal aperture and orbits (midfacial height) and relative midfacial prognathism. In addition, it displays an intermediate condition (between great apes and other anthropoids or the primitive condition for hominoids, as reconstructed here) for face shape and subnasal clivus length. In some cases, as for face shape, some other taxa (e.g., *Papio*) share the derived condition observed in hominids,

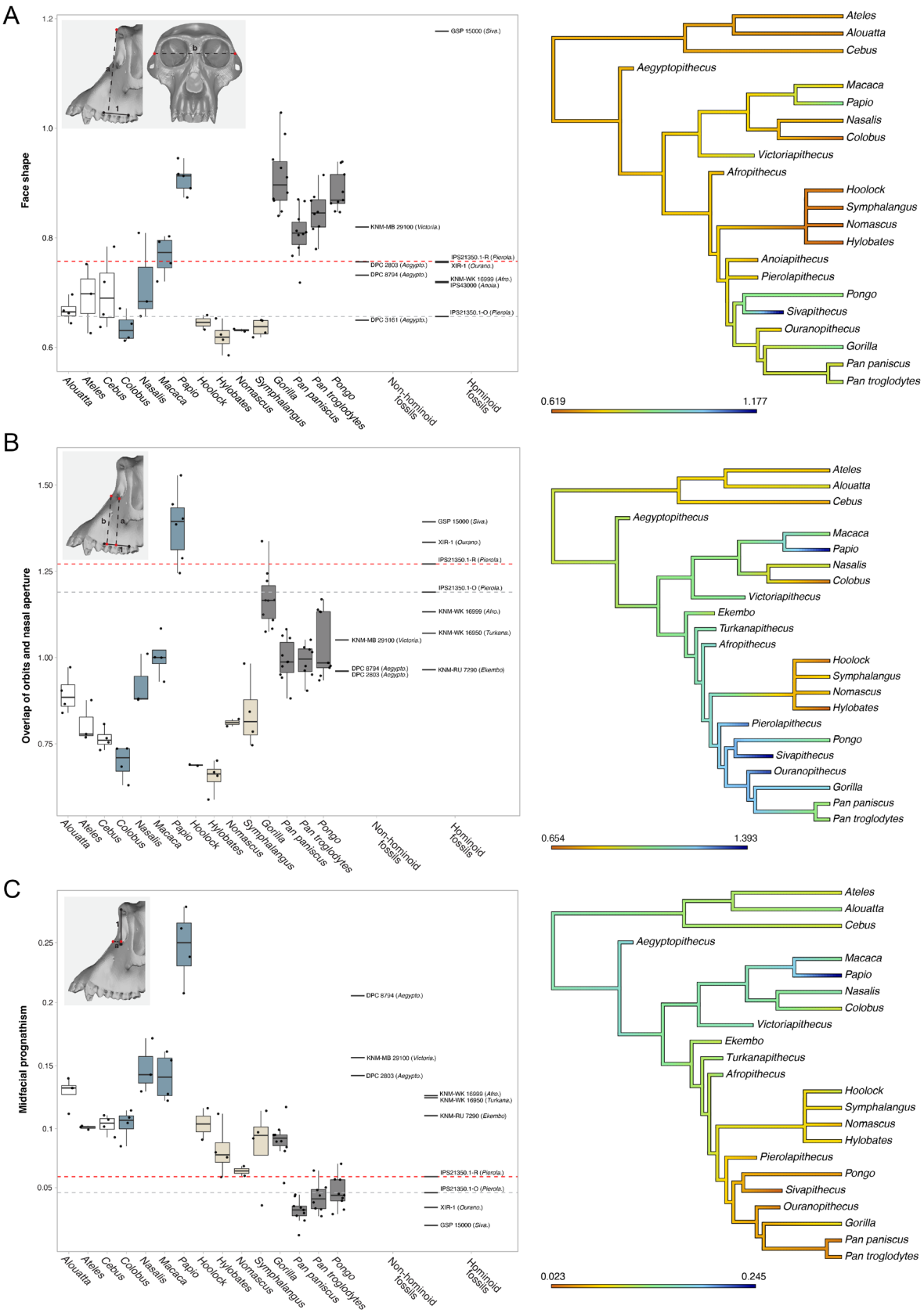

Fig. 5. Boxplots and phylogenetic trees showing ASRs for continuous features for extant and fossil anthropoids: (*A*) face shape (facial height [*A*-a] measured from the alveolar plane [*A*-1] divided by breadth [*A*-b]). (*B*) Superoinferior overlap of the orbits and nasal aperture (height of orbit [*B*-a] divided by height of rhinion [*B*-b], both measured from the alveolar plane [*B*-1]), and (*C*) midfacial prognathism (distance [*C*-a] between rhinion and a bi-orbital plane [*C*-1] divided by CS). *Pierolapithecus* is represented by the unreconstructed (O; gray dashed line) and reconstructed (R; red dashed line) cranium in each boxplot. The boxes represent the range between the first and third quartiles, with the median indicated by the horizontal line. The whiskers represent the largest and smallest values within 1.5 times the interquartile range. Colors on the phylogenetic trees represent the continuous character state for each feature, from the smallest (red) to largest (dark blue) value. See *Inset* crania in each panel and *SI Appendix*, Table S6 for details on how each feature was measured.

but the similarity is reconstructed as independently derived. In orbit shape and interorbital breadth, *Pierolapithecus* is distinct from the characteristic features of *Pongo* and more closely resembles many other hominoids in having a relatively wide interorbital breadth (*SI Appendix*, Fig. S17) and many anthropoids in having orbits that are slightly wider than tall (*SI Appendix*, Fig. S18). *Pierolapithecus* has a nasal aperture that is similar in relative breadth to the ranges of most monkeys, *Pongo*, and *Pan paniscus* (*SI Appendix*, Fig. S19). A moderately wide nasal aperture, slightly wider than in *Pierolapithecus*, is reconstructed as ancestral for hominids. A more vertical nasal aperture than observed in great apes or monkeys (with the exception of *Cebus*) is inferred for the hominoid and hominid nodes (*SI Appendix*, Fig. S20). Extant great apes overlap with *Symphalangus*, many monkeys, and the remaining fossil hominoids, including *Pierolapithecus*, for this feature. See *Extended Results* for more details.

Discussion

Pierolapithecus was described as having a "primitive hominoid facial profile" that is dorsoventrally low with a posteriorly situated glabella and nasals that form an acute angle with the palate (1:1,340). This arrangement was described as differing from Late Miocene and extant great apes, which have more orthognathic faces, and more closely resembling hylobatids and *Afropithecus*. In combination with these primitive features, *Pierolapithecus* was noted to have derived features interpreted as hominid synapomorphies (shared, derived features), including flat nasals that project anteriorly beneath the level of the lower orbital rims, an elevated zygomatic root, a deep palate, and a broad nasal aperture that is widest inferiorly (1). The virtual reconstruction of the *Pierolapithecus* holotype cranium performed here clarified many aspects of its anatomy, including the height and breadth of the face, the extent of prognathism, the orientation of the zygomatics, and the shape, size, and orientation of the orbits and nasal aperture. Overall, the reconstructed face has a relatively taller, more orthognathic appearance than the original, with a more anteriorly situated glabella and rhinion. This configuration results in a more vertical nasal aperture and orbits. Repositioning of the fragments of the orbital margin confirms that the orbits are slightly wider than tall, and the addition of the previously unpublished maxillary fragment reveals the shape and proportions of the nasal aperture. Despite these key differences, the reconstruction also substantiates the presence of facial synapomorphies that link *Pierolapithecus* with hominids noted in the original description (1) and allows for updated and quantitative comparisons of its morphological affinities to other anthropoids, particularly extant great apes and other ACM hominoids, and investigations of the morphological evolution of the hominid face.

Morphological Affinities of the *Pierolapithecus* Face. As noted above, *Pierolapithecus* shares a number of features with hominids to the exclusion of other hominoids, some of which were altered slightly by the reconstruction and evaluated quantitatively and using evolutionary modeling here for the first time. Low midfacial prognathism and orbits that sit above the nasal aperture were supported as derived features that link *Pierolapithecus* with hominids. Moderate midfacial prognathism characterizes all crown hominoids, while lower midfacial prognathism characterizes hominids including *Pierolapithecus* (2, 13, see also refs. 25 and 26). Reduced midfacial prognathism sets crown hominoids apart from Early Miocene hominoids from Africa, such as *Afropithecus*, *Turkanapithecus*, and *Ekembo*. Hominids are also characterized by a taller midface with less superoinferior overlap of the nasal aperture and orbits, although some other catarrhines, particularly those with longer muzzles like *Papio* and *Macaca*, also have taller midfaces. Still, an elongated midface with orbits that sit above the apex of the nasal aperture is reconstructed as a derived feature linking *Pierolapithecus* and hominids.

There are also several notable ways that *Pierolapithecus* differs from extant great apes. The latter are characterized by the overlap of the premaxilla and hard palate and elongation of the subnasal clivus (13, 27, 28), while a short clivus that does not overlap the palate has been inferred to be the ancestral state for hominoids (14, 29–35). Despite damage to the posterior end of the premaxilla, it is apparent that it would not have overlapped the hard palate in IPS21350.1 (17, 36) (*SI Appendix*, Fig. S21), and the subnasal clivus is abbreviated compared to that of extant great apes. The presence of a moderately elongated clivus in *Afropithecus* is likely to be convergent with hominids (following the phylogenetic hypothesis used here, in which this taxon is a stem hominoid). *Nacholapithecus*, a probable stem hominoid (17) or stem hominid (37) from the Middle Miocene of Africa, has also been reported to have an elongated clivus that overlaps the hard palate (35, 38), but the subnasal portion is quite abbreviated. Another feature in which *Pierolapithecus* differs from extant great apes is the relative height of the face. The reconstruction features a relatively taller face than the original specimen but one that is still superoinferiorly shorter than that of extant great apes and the reconstructed crown hominid node, despite clear elongation of the midface. Based on the distribution of these features in fossil hominids, extant great ape-like premaxilla/palate overlap, elongation of the subnasal clivus, and relatively tall faces characterize crown hominids, but not all stem members of the group, and therefore evolved sometime after the origin of the clade (see also ref. 17). Dentally, *Pierolapithecus* also retains a number of features that have been inferred to be primitive for hominids, including a prominent lingual pillar on the upper central incisors (20). Other features, such as molar enamel thickness, have been somewhat useful for taxonomic assessments but are more difficult to interpret in a higher-level phylogenetic context (21).

While it is broadly accepted that *Pierolapithecus* represents a hominid, and our results support this hypothesis, the question of its relationship to extant hominid subfamilies is more contentious (reviewed in ref. 11). Some authors interpret the features of *Pierolapithecus* as evidence for a position as a stem member of the clade (1, 16, 17). Alternatively, the possibility that *Pierolapithecus* represents a hominine (13, 39) or a pongine (10, 36) has also been raised. Extant pongines and hominines are morphologically distinct from one another in many aspects of their facial morphology. Orangutans (*Pongo*) are characterized by orbits that are taller than broad, a narrow interorbital pillar, smooth topography of the subnasal region, a very elongated subnasal clivus, supraorbital costae, anteriorly oriented zygomatic region, and a more vertically oriented frontal squama, among others; in contrast, African apes (*Gorilla* and *Pan*) are characterized by orbits that are as wide or wider than they are tall, a broad interorbital pillar, a stepped subnasal region, moderately to very elongated subnasal clivus, a supraorbital torus, laterally sloping zygomatic region, and a more horizontally oriented frontal squama (13, 25, 27, 29, 30, 33, 40–42). There are also notable differences in the internal morphology of the face, with *Pongo* having more restricted maxillary sinuses with frontal recesses and lacking pneumatization of the frontal bone, and *Gorilla* and *Pan* having larger maxillary sinuses and extensive frontal sinuses that have an ethmoid origin (43–45).

Despite the distinctiveness of pongines and hominines, disagreements remain about the affinities of many fossil hominoids because they have unique combinations of features and the

polarity of many of these features is subject to debate. For example, *Pongo* is often considered to be highly derived in many aspects of its cranial morphology, particularly in the orbital and subnasal regions (30, e.g., refs. 40 and 42), while other authors have suggested that some of these features (e.g., those of the orbital region) may be primitive for hominoids (e.g., refs. 46 and 47). This uncertainty is further compounded by the incomplete preservation of many fossil crania and differences of interpretation for the features that are preserved (e.g., of what constitutes a supraorbital torus/costae or the derivation of sinuses invading the frontal bone; see discussion in ref. 17). *Pierolapithecus* does not closely match the facial features of either hominines or pongines, having relatively wide orbits, a broad interorbital pillar, a premaxilla that does not overlap the palate, a short subnasal clivus, a supraorbital region that is distinct from both African ape-like tori and *Pongo*-like costae, a laterally sloping zygomatic region, and a more vertically oriented frontal squama. A previous investigation of the internal morphology of the face documented a restricted maxillary sinus and the absence of a sinus invading the frontal bone (36). In these features, *Pierolapithecus* is more similar to some pongines than to hominines, although it is difficult to resolve their polarity, and there is intraspecific variation in the size and shape of the paranasal sinuses (e.g., refs. 36, 45, 48–51). Thus, *Pierolapithecus* shares a selection of derived external facial features with hominids but notably lacks the full suite of features characteristic of crown members of the clade. It also lacks clear synapomorphies shared with either pongines or hominines that would indicate an exclusive relationship with one of these subfamilies. Taken together, this combination of features is most consistent with a phylogenetic position as a stem hominid, as has been previously suggested for *Pierolapithecus* (1, 17, 52).

In addition to assessing the affinities of *Pierolapithecus* to extant clades, the reconstruction also allows for a reevaluation of the similarities and differences of the three hominoid species represented at ACM (Fig. 6). The distinctiveness of *Pierolapithecus* from other ACM hominoids has been questioned, in part due to the distortion of known cranial specimens and the close temporal and spatial proximity of the fossils (13, 22, 23). However, a number of cranial and dental features have been used to differentiate *Anoiapithecus*, *Dryopithecus*, and *Pierolapithecus* from each other (2, 3, 18–21, 36, 53, 54 and *SI Appendix, Extended Discussion*) and, based on our results, *Pierolapithecus* and *Anoiapithecus* can also be distinguished from *Dryopithecus* in the superoinferior position of the orbits relative to the nasal aperture, the degree of midfacial prognathism, the breath of the nasal aperture, and (face) size (*SI Appendix, Extended Discussion*). Despite these noted differences, *Pierolapithecus* and *Anoiapithecus* are very close to each other (and to most other hominids) in the shape spaces derived from PCA analyses, perhaps reflecting their overall hominid-like morphology. However, while many of the cranial features noted to differentiate the ACM hominoids in previous studies are preserved in the reconstruction, it is more similar to *Anoiapithecus* and/or *Dryopithecus* in several ways. For example, the more orthognathic profile is more similar to, but still distinct from, *Anoiapithecus.* Altogether, we find the ACM

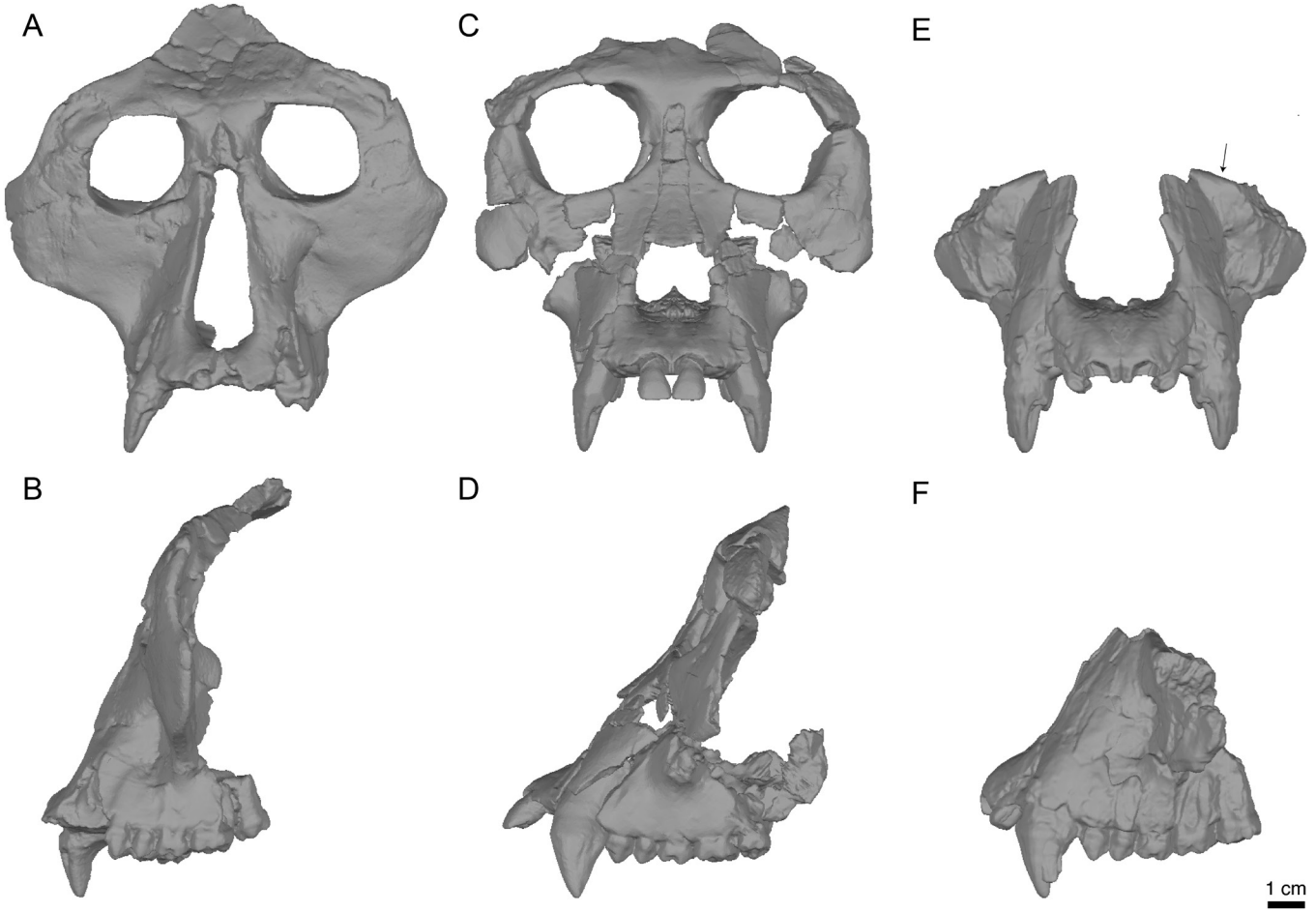

Fig. 6. Comparisons of ACM large-bodied hominoids in anterior and lateral views. (*A* and *B*) Reconstruction of *Anoiapithecus* (IPS43000) from Moyà-Solà et al. (2); (*C* and *D*) reconstruction of *Pierolapithecus* (IPS21350.1); (*E* and *F*) reconstruction of *Dryopithecus* (IPS35026; *SI Appendix*, Table S4). The black arrow indicates the preserved orbital margin in *Dryopithecus*.

hominoids to differ considerably in their craniofacial morphology and consider them to be sufficiently distinct to maintain three different genera.

Evolution of the Hominid Face. Besides important differences in postcranial morphology and body size, living great apes differ greatly from hylobatids in craniodental anatomy (17, 28, 55–57). This disparity, along with the paucity of stem hylobatids in the fossil record (58, 59), has made it difficult to unravel the evolutionary history of the hominoids and, in particular, the morphotype of the LCA of living hominoids from which both hominids and hylobatids evolved. On the other hand, although fragmentary, the fossil record of stem hominoids and hominids is more complete than that of hylobatids. Alongside extant hominoids, these fossils form the basis of efforts to determine which features characterize the ancestor of living hominoids. Stem members of the hominid lineage, like *Pierolapithecus*, are essential to elucidating the hominid and crown hominoid LCAs because they show combinations of primitive and derived features that may more closely resemble those present in these ancestors.

Based on the currently-limited fossil record, it has been proposed that living hominoids evolved from a LCA that was hylobatid-like in morphology and size (e.g., refs. 31, 52, 60–62). This is supported, in part, by cranial similarities among hylobatids, *Colobus*, and pliopithecoids, which are characterized by short snouts and globular neurocrania (31, 61). The stem hominoid *Nyanzapithecus* is also somewhat hylobatid-like in gross cranial form (63), as is *Pliobates* (52), a catarrhine of debated phylogenetic affinities (52, 63, 64) that does not preserve the full suite of landmarks and could not be included in the present study. Under this hypothesis, observations of morphological continuity between fossil hominoids from the Early and Middle Miocene have been interpreted as evidence that some Early Miocene taxa (e.g., *Morotopithecus*, *Afropithecus,* and/or *Proconsul* s.l.) are hominids (e.g., refs. 15, 28, 65–67). However, the discovery of cranial remains of the stem cercopithecoid *Victoriapithecus* and the stem hominoid *Afropithecus*, both of which resemble the stem catarrhine *Aegyptopithecus,* papionins, and (to a lesser degree) hominids in having long, lower crania with prognathic faces, resulted in a revision of ancestral catarrhine morphotypes (47, 67–72). Others have also suggested that the fossil evidence is more consistent with a larger-bodied, more great ape-like ancestral hominoid (55, 73, 74). Under this hypothesis, there is morphological continuity in cranial shape and size between stem hominoids and hominids that makes it difficult to distinguish them in the fossil record.

The reconstruction of *Pierolapithecus* and the analyses performed here lend insight into the morphological evolution of the hominoid face, with our results providing provisional support for the latter hypothesis. ASR of hominoid and hominid nodes in the 3D phylomorphospace (and several of the indices, such as relative face height) indicate that the ancestors of all hominoids, all crown hominoids, and all hominids were more similar to crown hominids than to hylobatids in face shape and size and that a hylobatid-like shape (i.e., superoinferiorly short face, extensive overlap of orbits and nasal aperture, relatively orthognathic face) emerged multiple times convergently throughout catarrhine evolution (in, e.g., *Colobus* and pliopithecoids). Our analyses indicate that homoplastic similarities in the face morphology of these taxa may be consequences of allometry related to independent reductions in body size (reflected in face CS; Fig. 4). These results, however, are sensitive to both phylogenetic uncertainty for fossil taxa and the addition of new, more complete stem hominoid fossils. When analyses were performed with a reduced landmark dataset to include *Ekembo*, the hominoid total group node was shifted slightly closer to hylobatids and monkeys.

Among anthropoids, great apes occupy their own shape space in the 3D phylomorphospace, even relative to stem hominoids (represented here by *Afropithecus* and, in the reduced landmark analyses, *Ekembo*), which are more great ape-like than hylobatid-like but pull out from the great ape cluster in the direction of cercopithecoids. Of the facial features investigated here, only midfacial prognathism distinguishes stem hominoids from the great apes in our sample. *Afropithecus* has several features (to varying degrees) for which hominids or crown hominids are reconstructed as derived, including moderate elongation of the subnasal clivus and orbits that sit above the nasal aperture. These features may be independently derived in *Afropithecus* or may be ancestral for crown hominoids, with hylobatids displaying a secondarily derived state. The latter explanation is supported by the evolutionary modeling performed here (which, again, is sensitive to the addition of fossils and the evolutionary model used). Other stem hominoids, aside from *Afropithecus*, do not have elongated subnasal clivi, lending support to the idea that increased fossil sampling may modify the ASR for this feature.

The LCA of all hominids has been posited to be *Pongo*-like (46, 47, 67, 71) or *Gorilla*-like (33, 75) in some features, while the analysis of the probable stem hominid *Sinopithecus hudienensis* revealed phenetic affinities to *Pan* that may be interpreted as primitive retentions in the latter taxon (42). In contrast, Moyà-Solà et al. (1:1,340) suggested that *Pierolapithecus*, which is distinct from living great apes in many ways, may represent a "good prototype" for the facial anatomy of early hominids. The combined results of our 2D and 3D analyses indicate that the LCA of all hominids is distinct from all three living great ape genera and from *Pierolapithecus* in overall cranial shape, but that it is similar to *Pierolapithecus* in several of the linear and angular features examined here. The latter result is perhaps not unexpected given the proximity of *Pierolapithecus* to the base of the hominid clade (i.e., its position as a stem hominid) in the phylogenetic hypothesis used to model the evolution of these features. However, the inferred position of the hominid node in the 3D phylomorphospace (Fig. 3) suggests that, in overall facial shape, the hominid LCA is perhaps closer to *Gorilla* or *Pongo* than to *Pan* or *Pierolapithecus*.

The results of the evolutionary modeling of linear and angular features indicate that the ancestral hominid can be expected to have the following features: a moderately tall face, low midfacial prognathism, a superoinferiorly elongated midface with orbits that sit above the nasal aperture, orbits that are taller than wide, a broad interorbital pillar, a relatively vertical and moderately broad nasal aperture that is broadest inferiorly, and a somewhat elongated subnasal clivus. Many of these features are also reflected in the warped mesh reconstructions of the LCA of all hominids based on 3D data (*SI Appendix*, Fig. S14). One notable difference between our reconstructions of the hominid LCA and *Pierolapithecus* is in orbit shape. *Pierolapithecus* has relatively broad orbits, while the reconstruction of the hominid LCA exhibits orbits that are taller than wide. As with all reconstructions of ancestral morphotypes, the fragmentary nature of the fossil record precludes a comprehensive assessment of many features. Thus, the reconstruction of the morphotype of the ancestral hominid is destined for revision as new fossils are discovered, particularly stem hominoids, stem hylobatids, and stem hominids, but the present analyses support a hominid ancestor that was distinct in overall shape from all extant and fossil hominids and similar in many features to *Pierolapithecus*.

Materials and Methods

CT Data Acquisition and Reconstruction. The holotype cranium of *Pierolapithecus* (IPS21350.1) is housed at the Institut Català de Paleontologia Miquel Crusafont (ICP) in Sabadell, Spain. The specimen was transported to Centro Nacional de Investigación

sobre la Evolución Humana (CENIEH, Burgos, Spain) for high resolutions scanning. Avizo (v. 7; FEI-Visualization Sciences Group Inc.) was used to visualize the CT images and to define and segment individual bone fragments. Each of the defined segments (Fig. 1 and *SI Appendix*, Fig. S22) was converted to PLY format and exported from Avizo into Geomagic Wrap (2021; 3D Systems), where the surfaces were smoothed and converted into surface models. The separated bone fragments were repositioned in Geomagic Wrap. See *SI Appendix*, *Extended Methods* for details and data sharing plan.

Comparative Sample and Phylogenetic Tree. The extant and fossil specimens included in the sample are listed in *SI Appendix*, Tables S3 and S4. Several fossil crania in the comparative sample were minimally reconstructed so that they could be included in the 3D geometric morphometric analyses (*SI Appendix*, Table S4 and *Extended Methods*). The phylogenetic tree was created using published molecular estimates for relationships and divergence dates among extant taxa (*SI Appendix*, Table S7). Extinct taxa were added to this tree based on previous phylogenetic hypotheses from the literature and their published age and/or position relative to major nodes, using standard ghost lineages of one million years (e.g., ref. 76; *SI Appendix*, Table S8 and *Extended Methods*). Additional taxa were added to this tree following (59, 63) to model M^1 size as a proxy for body size (*SI Appendix*, Fig. S15).

Geometric Morphometric Analyses. Shape data for 3D geometric morphometric analyses were obtained from raw coordinate data for 67 face landmarks (and a second reduced landmark dataset of 53 landmarks) that were subject to a generalized Procrustes analysis and visualized with PCA (of individual specimens and taxon means in the phylomorphospace). Phylogenetic signal was estimated using Blomberg's *K* (77) and Pagel's λ (78). *K* and λ measure the tendency of closely related species to resemble each other under a Brownian motion model of evolution. Values near zero indicate that there is no phylogenetic structure to the data, while values near one indicate high phylogenetic signal as expected under a Brownian motion model. A *K* greater than one indicates that species resemble each other more than is expected under a Brownian motion model. These values are sensitive to measurement error and sample size, especially when the evolutionary history of a trait follows Brownian motion (77, 79). 3D landmarks were placed in Landmark Editor (v3.0; 80). 3D geometric morphometric analyses and modeling of these data were carried out in "geomorph" (v.4.0.2; 81, 82) "phytools" (v.1.0–3; 83) in R (v.4.1.2; 84); the PGLS regression was carried out in "caper" (v.1.0.1; 85).

3D visualization of ancestral shape at the hominid node was conducted by warping 3D meshes of extant members of the clade (*Gorilla*, *Pan*, and *Pongo*) into the shapes defined by the ancestral landmark coordinates. The complete analysis required the use of functions from the following packages: "Morpho" (v.2.10; 86), "ape" (v.5.6–2; 87), "phytools," and "geomorph". Ancestral shape at the hominid node was reconstructed using ML. Cluster analyses were performed in "phanghorn" (v.2.8.1; 88) based on two different matrices: i) a distance matrix generated from Procrustes distances and ii) a distance matrix generated by summing up the matrix of Procrustes distances and a matrix of Euclidean distances between lnCS values, both rescaled between 0 and 1.

Other Continuous Facial Traits. Linear distances were extracted from landmark data or measured in Geomagic Wrap; angles were measured in Geomagic Wrap by defining lines and/or planes and measuring the angle between them (*SI Appendix*, Table S6). Features were visualized using boxplots and evolutionary modeling (ASR) was performed in "phytools". The same methods were used to model M^1 size. For linear indices, the two variables of each index were also modeled separately to ensure that similarity in index values was not driven by independent change in the numerator or denominator; see *SI Appendix*, *Extended Methods* and Fig. S23). The phylogenetic signal for each trait was calculated using Blomberg's *K* and Pagel's λ in phytools.

Data, Materials, and Software Availability. Reconstruction and segmentation surface models data have been deposited in MorphoSource (https://www.morphosource.org/projects/000472979) (89). All other data are included in the article and/or supporting information. Some study data available (Surface models are openly available. CT raw data are available upon request via MorphoSource for research purposes following the same guidelines as for physical fossils housed in the ICP).

ACKNOWLEDGMENTS. MicroCT scanning of IPS21350.1 was performed at CENIEH facilities with the collaboration of CENIEH staff (Belén Notario). We acknowledge A. Serrano Martínez for transport and facilitation of the scanning. Thanks to A. Anaya, M. Biernat, E. Cordiner, S. Israelsson, K. Lauria, S. Nyandwi, R. Sherwood, N. Toews, and D. Wawrzyniak for 3D scanning and data processing assistance and to V. Vinuesa for data processing and assisting with landmark data collection. We are grateful for K. Chapelle's help with image processing software. Thanks to E. Delson and the New York Consortium in Evolutionary Primatology (NYCEP) scan database for access to casts and for providing the scan of *Victoriapithecus*, and to M. Tocheri and E. Gilissen for sharing scans of extant apes. L. Copes, L. Lucas, and the Museum of Comparative Zoology provided access to scans for MCZ 38018 (DOI: 10.17602/M2/M4399), MCZ 38019 (DOI: 10.17602/M2/M4398), MCZ 38020 (DOI: 10.17602/M2/M4397), and MCZ 31619 (DOI: 10.17602/M2/M4892). These scans were downloaded from MorphoSource. The Duke Lemur Center (DLC), Division of Fossil Primates granted access to the three *Aegyptopithecus* specimens via MorphoSource: DPC 2803 and DPC 3161, the collection of which was funded by NSF BCS 1231288 (to E.R. Seiffert, G. F. Gunnell, D. M. Boyer, and J. G. Fleagle) and NSF DBI 1458192 (to G. F. Gunnell, R. F. Kay and D. M. Boyer), and DPC 8794, the collection of which was funded by NSF DBI 2023087. This work is part of R+D+I projects PID2020-116908GB-I00, PID2020-117289GB-I00, PID2020-117118GB-I00, funded by the Agencia Estatal de Investigación (AEI) of the Ministerio de Ciencia e Innovación (MCIN) from Spain (MCIN/AEI/10.13039/501100011033/), and it has been further supported by the Generalitat de Catalunya/CERCA Programme (Research Centres of Catalonia) and research support grants (SGR) of the Agència de Gestió d'Ajuts Universitaris i de Recerca (Generalitat de Catalunya) to consolidated research groups (2021 SGR 01184, 2021 SGR 01188, and 2021 SGR 00620). S.A.C. is supported by BID PICT 2019-03675 and J.F. is supported by a Ramón y Cajal grant [RYC2021-032857-I] financed by MCIN/AEI/10.13039/501100011033 and the European Union "NextGenerationEU"/PRTR. This is NYCEP Morphometrics Contribution #120.

Author affiliations: [a]Department of Anthropology, Brooklyn College, City University of New York, Brooklyn, NY 11210; [b]Division of Anthropology, American Museum of Natural History, New York, NY 10024; [c]New York Consortium in Evolutionary Primatology, New York, NY 10024; [d]Unidad Ejecutora Lillo, Consejo Nacional de Investigaciones Científicas y Técnicas—Fundación Miguel Lillo, San Miguel de Tucumán 4000, Argentina; [e]Facultad de Ciencias Naturales e Instituto Miguel Lillo, Universidad Nacional de Tucumán, San Miguel de Tucumán 4000, Argentina; [f]Unidad de Antropología física, Departamento de Biodiversidad, Ecología y Evolución, Facultad de Ciencias Biológicas, Universidad Complutense de Madrid, Madrid 28040, Spain; [g]Institut Català de Paleontologia Miquel Crusafont, Universitat Autònoma de Barcelona, Barcelona 08193, Spain; [h]Department of Cell Biology, New York University Grossman School of Medicine, New York, NY 10016; [i]Department of Foundations of Medicine, New York University Long Island Grossman School of Medicine, Mineola, NY 11501; [j]Richard Gilder Graduate School, American Museum of Natural History, New York, NY 10024; [k]Institució Catalana de Recerca i Estudis Avançats, Barcelona 08010, Spain; and [l]Unitat d'Antropologia Biològica, Departament de Biologia Animal, Biologia Vegetal i Ecologia, Universitat Autònoma de Barcelona, Barcelona 08193, Spain

1. S. Moyà-Solà, M. Köhler, D. M. Alba, I. Casanovas-Vilar, J. Galindo, *Pierolapithecus catalaunicus*, a new middle miocene great ape from Spain. *Science* **306**, 1339–1344 (2004).
2. S. Moyà-Solà *et al.*, A unique Middle Miocene European hominoid and the origins of the great ape and human clade. *Proc. Natl. Acad. Sci. U.S.A.* **106**, 9601–9606 (2009).
3. S. Moyà-Solà *et al.*, First partial face and upper dentition of the Middle Miocene hominoid *Dryopithecus fontani* from Abocador de Can Mata (Vallès-Penedès Basin, Catalonia, NE Spain): Taxonomic and phylogenetic implications. *Am. J. Phys. Anthropol.* **139**, 126–145 (2009).
4. M. Böhme *et al.*, A new Miocene ape and locomotion in the ancestor of great apes and humans. *Nature* **575**, 489–493 (2019).
5. S. Almécija, D. M. Alba, S. Moyà-Solà, *Pierolapithecus* and the functional morphology of Miocene ape hand phalanges: Paleobiological and evolutionary implications. *J. Hum. Evol.* **57**, 284–297 (2009).
6. A. S. Hammond, D. M. Alba, S. Almécija, S. Moyà-Solà, Middle Miocene *Pierolapithecus* provides a first glimpse into early hominid pelvic morphology. *J. Hum. Evol.* **64**, 658–666 (2013).
7. D. M. Alba, S. Almécija, S. Moyà-Solà, Locomotor inferences in *Pierolapithecus* and *Hispanopithecus*: Reply to Deane and Begun (2008). *J. Hum. Evol.* **59**, 143–149 (2010).
8. A. Deane, D. R. Begun, Broken fingers: Retesting locomotor hypotheses for fossil hominoids using fragmentary proximal phalanges and high-resolution polynomial curve fitting (HR-PCF). *J. Hum. Evol.* **55**, 691–701 (2008).
9. S. Almécija, J. B. Smaers, W. L. Jungers, The evolution of human and ape hand proportions. *Nat. Commun.* **6**, 7717 (2015).
10. D. M. Alba, Fossil apes from the Vallès-Penedès basin. *Evol. Anthropol.* **21**, 254–269 (2012).
11. S. Almécija *et al.*, Fossil apes and human evolution. *Science* **372**, eabb4363 (2021).

12. D. R. Begun, C. V. Ward, M. D. Rose, "Events in hominoid evolution" in *Function, Phylogeny, and Fossils: Miocene Hominoid Evolution and Adaptations*, D. R. Begun, C. V. Ward, M. D. Rose, Eds. (Springer, 1997), pp. 389–415.
13. D. R. Begun, M. C. Nargolwalla, L. Kordos, European Miocene Hominids and the origin of the African ape and human clade. *Evol. Anthropol.* **21**, 10–23 (2012).
14. S. Moyà-Solà, M. Köhler, New partial cranium of *Dryopithecus* lartet, 1963 (Hominoidea, Primates) from the upper Miocene of Can Llobateres, Barcelona, Spain. *J. Hum. Evol.* **29**, 101–139 (1995).
15. P. J. Andrews, Evolution and environment in the hominoidea. *Nature* **360**, 641–646 (1992).
16. T. Harrison, Apes among the tangled branches of human origins. *Science* **327**, 532–534 (2010).
17. K. D. Pugh, Phylogenetic analysis of Middle-Late Miocene apes. *J. Hum. Evol.* **165**, 103140 (2022).
18. D. M. Alba *et al.*, New dental remains of *Anoiapithecus* and the first appearance datum of hominoids in the Iberian Peninsula. *J. Hum. Evol.* **65**, 573–584 (2013).
19. D. M. Alba *et al.*, A new dryopithecine mandibular fragment from the middle Miocene of Abocador de Can Mata and the taxonomic status of '*Sivapithecus*' *occidentalis* from Can Vila (Vallès-Penedès Basin, NE Iberian Peninsula). *J. Hum. Evol.* **145**, 102790 (2020).
20. M. Pérez de los Ríos, D. M. Alba, S. Moyà-Solà, Taxonomic attribution of the La Grive hominoid teeth. *Am. J. Phys. Anthropol.* **151**, 558–565 (2013).
21. J. Fortuny, C. Zanolli, F. Bernardini, C. Tuniz, D. M. Alba, Dryopithecine palaeobiodiversity in the Iberian Miocene revisited on the basis of molar endostructural morphology. *Palaeontology* **64**, 531–554 (2021).
22. D. R. Begun, Dryopithecins, Darwin, de Bonis, and the European origin of the African apes and human clade. *Geodiversitas* **31**, 789–816 (2009).
23. D. R. Begun, "Fossil record of miocene hominoids" in *Handbook of Paleoanthropology*, W. Henke, I. Tattersall, Eds. (Springer, Berlin Heidelberg, 2015), pp. 1261–1332.
24. D. R. Pilbeam, New hominoid skull material from the Miocene of Pakistan. *Nature* **295**, 232–234 (1982).
25. D. R. Begun, E. Güleç, Restoration of the type and palate of *Ankarapithecus meteai*: Taxonomic and phylogenetic implications. *Am. J. Phys. Anthropol.* **105**, 279–314 (1998).
26. L. Kordos, D. R. Begun, A new cranium of *Dryopithecus* from Rudabánya, Hungary. *J. Hum. Evol.* **41**, 689–700 (2001).
27. S. C. Ward, W. H. Kimbel, Subnasal alveolar morphology and the systematic position of *Sivapithecus*. *Am. J. Phys. Anthropol.* **61**, 157–171 (1983).
28. T. C. Rae, "The early evolution of the hominoid face" in *Function, Phylogeny, and Fossils: Miocene Hominoid Evolution and Adaptations*, D. R. Begun, C. V. Ward, M. D. Rose, Eds. (Springer, 1997), pp. 59–78.
29. S. C. Ward, D. R. Pilbeam, "Maxillofacial morphology of Miocene hominoids from Africa and Indo-Pakistan" in *New Interpretations of Ape and Human Ancestry*, R. L. Ciochon, R. S. Corrucini, Eds. (Springer, 1983), pp. 211–238.
30. S. C. Ward, B. Brown, "The facial skeleton of *Sivapithecus indicus*" in *Comparative Biology of Primates, Vol 1, Systematics, Evolution and Anatomy*, D. R. Swindler, J. Erwin, Eds. (Alan R. Liss, 1986), pp. 413–452.
31. T. Harrison, The phylogenetic relationships of the early catarrhine primates: A review of the current evidence. *J. Hum. Evol.* **16**, 41–80 (1987).
32. M. A. McCollum, F. E. Grine, S. C. Ward, W. Kimbel, Subnasal morphological variation in extant hominoids and fossil hominids. *J. Hum. Evol.* **24**, 87–111 (1993).
33. D. R. Begun, Relations among the great apes and humans: New interpretations based on the fossil great ape *Dryopithecus*. *Am. J. Phys. Anthropol.* **37**, 11–63 (1994).
34. B. Brown, J. Kappelman, S. Ward, "Lots of faces from different places: What craniofacial morphology does(n't) tell us about hominoid phylogenetics" in *Interpreting the Past: Essays on Human, Primate and Mammal Evolution in Honor of David Pilbeam*, D. E. Lieberman, R. J. Smith, J. Kelley, Eds. (Brill Academic Publishers, 2005), pp. 167–188.
35. M. Nakatsukasa, Y. Kunimatsu, *Nacholapithecus* and its importance for understanding hominoid evolution. *Evol. Anthropol.* **18**, 103–119 (2009).
36. M. Pérez de los Ríos, S. Moyà-Solà, D. M. Alba, The nasal and paranasal architecture of the Middle Miocene ape *Pierolapithecus catalaunicus* (primates: Hominidae): Phylogenetic implications. *J. Hum. Evol.* **63**, 497–506 (2012).
37. Y. Kunimatsu, M. Nakatsukasa, D. Shimizu, Y. Nakano, H. Ishida, Loss of the subarcuate fossa and the phylogeny of *Nacholapithecus*. *J. Hum. Evol.* **131**, 22–27 (2019).
38. H. Ishida, Y. Kunimatsu, T. Takano, Y. Nakano, M. Nakatsukasa, *Nacholapithecus* skeleton from the Middle Miocene of Kenya. *J. Hum. Evol.* **46**, 69–103 (2004).
39. D. R. Begun, C. V. Ward, Comment on "*Pierolapithecus catalaunicus*, a New Middle Miocene great ape from Spain". *Science* **308**, 203c (2005).
40. P. J. Andrews, J. E. Cronin, The relationships of *Sivapithecus* and *Ramapithecus* and the evolution of the orang-utan. *Nature* **297**, 541–546 (1982).
41. B. Brown, S. C. Ward, "Basicranial and facial topography in *Pongo* and *Sivapithecus*" in *Orang-utan Biology*, J. H. Schwartz, Ed. (Oxford University Press, 1988), pp. 247–260.
42. J. Kelley, F. Gao, Juvenile hominoid cranium from the late Miocene of southern China and hominoid diversity in Asia. *Proc. Natl. Acad. Sci. U.S.A.* **109**, 6882 (2012).
43. A. J. E. Cave, R. W. Haines, The paranasal sinuses of the anthropoid apes. *J. Anat.* **74**, 493–523 (1940).
44. T. Koppe, Y. Okhawa, "Pneumatization of the facial skeleton in catarrhine primates" in *The Paranasal Sinuses of Higher Primates: Development, Function, and Evolution*, T. Koppe, H. Nagai, K.W. Alt, Eds. (Quintessence, 1999), pp. 77–119.
45. J. B. Rossie, The phylogenetic significance of anthropoid paranasal sinuses. *Anat. Rec.* **291**, 1485–1498 (2008).
46. R. E. F. Leakey, A. Walker, New higher primates from the early Miocene of Buluk, Kenya. *Nature* **318**, 173–175 (1985).
47. B. R. Benefit, *Victoriapithecus*: The key to Old World monkey and catarrhine origins. *Evol. Anthropol.* **7**, 155–174 (1999).
48. T. C. Rae, T. Koppe, Holes in the head: Evolutionary interpretations of the paranasal sinuses in catarrhines. *Evol. Anthropol.* **13**, 211–223 (2004).
49. A. Balzeau, L. Albessard-Ball, A. M. Kubicka, C. Noûs, L. T. Buck, Frontal sinus variation in extant species of the genera *Pan*, *Gorilla* and *Homo*. *BMSAP* **33**, 27–50 (2021).
50. C. P. E. Zollikofer, M. S. Ponce de León, R. W. Schmitz, C. B. Stringer, New insights into Mid-Late Pleistocene fossil hominin paranasal sinus morphology. *Anat. Rec.* **291**, 1506–1516 (2008).
51. J. Kappelman, B. G. Richmond, E. R. Seiffert, A. M. Maga, T. M. Ryan, "Hominoidea (Primates)" in *Geology and Paleontology of the Miocene Sinap Formation, Turkey*, M. Fortelius, J. Kappelman, S. Sen, R. L. Bernor, Eds. (Columbia University Press, 2003), pp. 90–124.
52. D. M. Alba *et al.*, Miocene small-bodied ape from Eurasia sheds light on hominoid evolution. *Science* **350**, aab2625 (2015).
53. D. M. Alba, J. Fortuny, S. Moyà-Solà, Enamel thickness in the Middle Miocene great apes *Anoiapithecus*, *Pierolapithecus* and *Dryopithecus*. *Proc. Biol. Sci.* **277**, 2237–2245 (2010).
54. C. Zanolli *et al.*, A reassessment of the distinctiveness of dryopithecine genera from the Iberian Miocene based on enamel-dentine junction geometric morphometric analyses. *J. Hum. Evol.* **177**, 103326 (2023).
55. T. C. Rae, Miocene hominoid craniofacial morphology and the emergence of great apes. *Ann. Anat.* **186**, 417–421 (2004).
56. S. G. Larson, Parallel evolution in the hominoid trunk and forelimb. *Evol. Anthropol.* **6**, 87–99 (1998).
57. N. M. Young, *Homology and Homoplasy in the Evolution of the Hominoid Postcranium* (Harvard University, Cambridge, M.A., 2002).
58. T. Harrison, "The fossil record and evolutionary history of hylobatids" in *Evolution of Gibbons and Siamang*, U. H. Reichard, H. Hirai, C. Barelli, Eds. (Springer, US, 2016), pp. 91–110.
59. C. C. Gilbert *et al.*, New Middle Miocene ape (Primates: Hylobatidae) from Ramnagar, India fills major gaps in the hominoid fossil record. *Proc. Biol. Sci.* **287**, 20201655 (2020).
60. A. Keith, Hunterian lectures on man's posture: Its evolution and disorders. *Br. Med. J.* **1**, 451–454 (1923).
61. E. Delson, P. J. Andrews, "Evolution and Interrelationships of the Catarrhine Primates" in *Phylogeny of the Primates*, W. P. Luckett, F. S. Szalay, Eds. (Springer, 1975), pp. 405–446.
62. M. Grabowski, W. L. Jungers, Evidence of a chimpanzee-sized ancestor of humans but a gibbon-sized ancestor of apes. *Nat. Commun.* **8**, 1–10 (2017).
63. I. Nengo *et al.*, New infant cranium from the African Miocene sheds light on ape evolution. *Nature* **548**, 169–174 (2017).
64. A. Urciuoli, D. M. Alba, Systematics of Miocene apes: State of the art of a neverending controversy. *J. Hum. Evol.* **175**, 103309 (2023).
65. P. J. Andrews, L. Martin, Cladistic relationships of extant and fossil hominoids. *J. Hum. Evol.* **16**, 101–118 (1987).
66. A. Walker, M. Teaford, The hunt for *Proconsul*. *Sci. Am.* **260**, 76–82 (1989).
67. B. R. Benefit, M. L. McCrossin, Ancestral facial morphology of Old World higher primates. *Proc. Natl. Acad. Sci. U.S.A.* **88**, 5267–5271 (1991).
68. R. E. Leakey, M. G. Leakey, A new hominoid from Kenya. *Nature* **324**, 143–146 (1986).
69. R. E. Leakey, M. G. Leakey, A. C. Walker, Morphology of *Afropithecus turkanensis* from Kenya. *Am. J. Phys. Anthropol.* **76**, 289–307 (1988).
70. M. G. Leakey, R. E. Leakey, J. T. Richtsmeier, E. L. Simons, A. C. Walker, Similarities in *Aegyptopithecus* and *Afropithecus* facial morphology. *Folia Primatol.* **56**, 65–85 (1991).
71. B. R. Benefit, M. L. McCrossin, Facial anatomy of *Victoriapithecus* and its relevance to the ancestral cranial morphology of Old World monkeys and apes. *Am. J. Phys. Anthropol.* **92**, 329–370 (1993).
72. B. R. Benefit, M. L. McCrossin, Earliest known Old World monkey skull. *Nature* **388**, 368–371 (1997).
73. D. R. Pilbeam, N. M. Young, Hominoid evolution: Synthesizing disparate data. *C. R. Palevol.* **3**, 305–321 (2004).
74. N. M. Young, L. M. MacLatchy, The phylogenetic position of *Morotopithecus*. *J. Hum. Evol.* **46**, 163–184 (2004).
75. D. R. Begun, Miocene fossil hominids and the chimp-human clade. *Science* **257**, 1929–1933 (1992).
76. S. Almécija *et al.*, Early anthropoid femora reveal divergent adaptive trajectories in catarrhine hind-limb evolution. *Nat. Commun.* **10**, 4778 (2019).
77. S. P. Blomberg, T. Garland Jr., A. R. Ives, Testing for phylogenetic signal in comparative data: Behavioral traits are more labile. *Evolution* **57**, 717–745 (2003).
78. M. Pagel, Inferring the historical patterns of biological evolution. *Nature* **401**, 877–884 (1999).
79. T. Münkemüller *et al.*, How to measure and test phylogenetic signal. *Methods Ecol. Evol.* **3**, 743–756 (2012).
80. D. F. Wiley, *Landmark Editor 3.0. Institute for Data Analysis and Visualization* (University of California, Davis, 2006).
81. D. C. Adams, M. Collyer, A. Kaliontzopoulou, E. Sherratt, Geomorph: Software for geometric morphometric analyses, v4.0.2. (2022). https://cran.r-project.org/package=geomorph.
82. E. K. Baken, M. L. Collyer, A. Kaliontzopoulou, D. C. Adams, Geomorph v4. 0 and gmShiny: Enhanced analytics and a new graphical interface for a comprehensive morphometric experience. *Methods Ecol. Evol.* **12**, 2355–2363 (2021).
83. L. J. Revell, phytools: An R package for phylogenetic comparative biology (and other things). *Methods Ecol. Evol.* **2**, 217–223 (2012).
84. R Core Team, R: A Language and Environment for Statistical Computing (R Foundation for Statistical Computing, Vienna, Austria, 2021), https://www.R-project.org/.
85. D. Orme, Caper: Comparative Analyses of Phylogenetics and Evolution in R, v1.0.1. (2018). https://cran.r-project.org/web/packages/caper/vignettes/caper.pdf.
86. S. Schlager, "Morpho and Rvcg–shape analysis in R: R-packages for geometric morphometrics, shape analysis and surface manipulations" in *Statistical Shape and Deformation Analysis*, G. Zheng, S. Li, G. Székely, Eds. (Elsevier, 2017), pp. 217–256.
87. E. Paradis, K. Schliep, ape 5.0: An environment for modern phylogenetics and evolutionary analyses in R. *Bioinformatics* **35**, 526–528 (2019).
88. K. P. Schliep, phangorn: Phylogenetic analysis in R. *Bioinformatics* **27**, 592–593 (2011).
89. K. D. Pugh *et al.*, Data for The reconstructed cranium of *Pierolapithecus* and the evolution of the great ape face. MorphoSource. https://www.morphosource.org/projects/000472979. Accessed 3 November 2022.